THE JOURNAL OF PHYSICAL CHEMISTRY C

pubs.acs.org/JPCC Article

Polarity- and Pressure-Dependent Hydrogen Dynamics on ZnO Polar Surfaces Revealed by Near-Ambient-Pressure X-ray Photoelectron Spectroscopy

Zhirui Ma, Ke Yang, Xu Lian, Shuo Sun, Chengding Gu, Jia Lin Zhang, Damien West, Shengbai Zhang, Lei Liu, Kaidi Yuan,* Yi-Yang Sun,* Hexing Li, and Wei Chen*

Cite This: J. Phys. Chem. C 2020, 124, 25431−25436 Read Online

ACCESS | Metrics & More | Article Recommendations | Supporting Information

ABSTRACT: ZnO-based catalysts have been widely used in industrial reactions involving syngas conversions. Hydrogen dynamics on the surface of the catalyst is an essential process for understanding the mechanisms of such reactions. As a polar material, however, the role of ZnO surface polarity on hydrogen dynamics has not been studied under operando conditions. Here, we investigate the behavior of polar (0001) and (000$\bar{1}$) surfaces of single-crystal ZnO under different H_2 pressures using near-ambient-pressure X-ray photoelectron spectroscopy. We found that the (000$\bar{1}$) surface shows a monotonic and irreversible band bending with increasing H_2 pressure. In contrast, the (0001) surface shows two opposite responses depending on H_2 pressure, which are reversible in pressure cycles. This polarity- and pressure-dependent hydrogen dynamics is clearly understood with the assistance from first-principles calculations. In particular, the amphoteric behavior of atomic H is identified to play a key role.

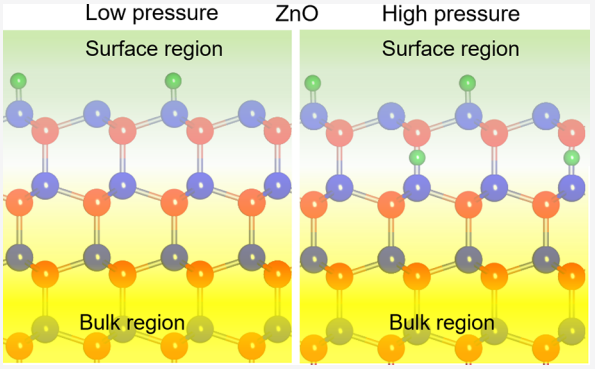

INTRODUCTION

Metal oxides constitute the largest family of catalysts in heterogeneous catalysis, either as supports or active phases.[1,2] ZnO has received significant attention in recent years because of its identified activity in a number of important catalytic reactions, such as methanol synthesis from syngas,[3,4] reverse water−gas shift reaction (rWGS)[5] and hydrogenation of syngas to light olefins.[6] ZnO is considered as a promoter and support in the Cu/ZnO catalyst to activate CO_2/CO followed by hydrogenation in rWGS and methanol synthesis. Although the hydrogenation of CO_2 and CO has been widely studied by experimental and theoretical methods,[3−5,7] the underlaying mechanism of these two reactions is yet to be further elaborated. For the synthesis of light olefins, it is reported that ZnO plays a key role in activating H_2 and CO,[6] while how H_2 interacts with ZnO still remains elusive. To understand the reaction mechanism of hydrogenation, revealing the interaction of H_2 with ZnO is necessary as it is the key step in the catalytic processes.

Previous studies focusing on the behavior of H_2 on ZnO single-crystal surfaces were summarized in a comprehensive review.[8] For the nonpolar ZnO (10$\bar{1}$0) surface, the exposure of atomic H at room temperature leads to the adsorption of H on surface O, which results in the formation of a metallic surface.[9] For polar surfaces like the ZnO (000$\bar{1}$) surface, the formation of the H-terminated surface is observed under atomic H atmosphere.[10] The interaction of H atoms with the ZnO (0001) surface is expected to be the weakest among all the ZnO surfaces, as the binding energy of the O−H bond is considerably higher than that of the Zn−H bond. The He-atom scattering study reveals the formation of Zn hydride species by a small dosage of atomic H to the ZnO (0001) surface.[11] Larger exposure of atomic H leads to a complete loss of the surface periodicity, as revealed by the scanning tunneling microscopy study.[12]

While the studies under ultrahigh vacuum (UHV) condition provide important clues, it is of greater relevance to reveal the catalytic mechanism under operando conditions, in particular, under ambient pressure, which has direct influence on the catalytic activity.[13−15] In the case of ZnO, feed gas strongly affects the morphology of the ZnO surface.[12] For the H_2 molecules on ZnO surfaces, the adsorption rate was reported below 1×10^{-6} under 1×10^{-6} mbar gas pressure at 200 K,[11] indicating that it is impossible to detect the adsorption of H_2

Received: September 30, 2020
Revised: October 22, 2020
Published: November 6, 2020

https://dx.doi.org/10.1021/acs.jpcc.0c08881
J. Phys. Chem. C 2020, 124, 25431−25436

molecules on the ZnO surface under UHV condition. Therefore, the atomic H is normally used to study the interaction of hydrogen with ZnO in the previous works.[9,16,17] These studies clearly demonstrated that the gaseous conditions can significantly affect the catalytic activity. Thus, the investigation of a well-defined model catalyst under near ambient pressure is crucial for the understanding of the interaction between H_2 and ZnO.

In this paper, we develop a sensitive method to detect surface species at a low coverage [below the detecting limit of X-ray photoelectron spectroscopy (XPS)]. With this method, even the hydrogen species could be indirectly detected. We use near-ambient-pressure XPS (NAP-XPS) to investigate the pressure-dependent core-level peak shifts, which are an indication of surface band bending. With this approach, we systematically study the interaction between hydrogen and ZnO polar surfaces with opposite polarity. Combining with density functional theory (DFT) calculations, we provide evidence for the essential role of ZnO in the activation of H_2. The H_2 molecules first undergo catalytic dissociation on the ZnO polar surfaces. The atomic H is adsorbed on the surfaces under low pressure and then diffuses into the ZnO(0001) subsurface to form interstitial hydrogen under high pressure. All these processes are dynamic and pressure-sensitive; therefore, they can only be captured by operando techniques like NAP-XPS. Our study not only reveals the distinct behaviors of the two polar surfaces of ZnO but also provides a direct evidence on the catalytic activity of ZnO surfaces toward H_2 molecules under realistic reaction conditions.

EXPERIMENTAL PROCEDURES

Sample Preparation and NAP-XPS Experiments. The experiments were carried out in a custom-designed NAP-XPS system, which is equipped with an analysis chamber (base pressure = 5×10^{-10} mbar) and a preparation chamber (base pressure below 6×10^{-11} mbar). The examination of carbon concentration (XPS) was carried out in the analysis chamber under UHV. The NAP-XPS experiments were carried out with a NAP-cell, which was inside but isolated from the analysis chamber.

The single-crystal ZnO samples were mounted on a molybdenum plate *via* tantalum strips. A number of sputtering−annealing cycles were carried out to clean the ZnO surfaces in the preparation chamber. The concentration of carbon was reduced below the detection limit of XPS. The gas dosage was through a gas line connected to the NAP cell and controlled by a precise leak valve. Special care was taken to prevent water contamination during the measurement: The analysis chamber, NAP cell, and gas line were thoroughly baked for degassing before the experiment, and freeze−pump−thaw cycles using liquid nitrogen trap were applied to prevent contamination during the measurement.

All the XPS spectra were collected *via* the Al Kα source (Specs, XR 50) with a passing energy of 20 eV at room temperature. The binding energies of the XPS spectra were calibrated by the Au 4f binding energy of a sputter-cleaned Au(111) sample. CaseXPS was used to analyze the XPS spectra which were fitted using the Shirley background and GL (70) line shape.

Theoretical Calculations. DFT calculations were performed with plane-wave basis and projector augmented wave[18] potentials as implemented in Vienna Ab Initio Simulation Package (VASP) code.[19,20] The generalized gradient approximation of Perdew, Burke, and Ernzerhof revised for solids (PBEsol) was used for the exchange−correlation functional.[21] The kinetic energy cutoff of plane-wave basis was 400 eV. Brillouin zone integration was performed on a Γ-centered 3 × 3×1 *k*-point grid. The 3 × 3 stoichiometric ZnO(0001)/$(000\bar{1})$ surface slabs containing 10 atomic layers, 45 O atoms and 45 Zn atoms were used to investigate the absorbed properties of H on the ZnO surface, and 2 × 2 ZnO(0001) was used to invesitigate the band structures. The four bottom layers were fixed at the bulk positions. To avoid charge transfer between two surfaces, the O dangling bonds on the $(000\bar{1})$ surface were passivated by pseudo-hydrogens (pseudo-H) with 0.5 valence electrons for investigating H on ZnO(0001), and Zn dangling bonds on the (0001) surface were passivated by pseudo-H with 1.5 valence electrons for investigating H on $(000\bar{1})$, respectively. In the structural relaxation, total energy and forces on all unfixed atoms were converged to less than 10^{-6} eV and 0.03 eV/Å, respectively. The vacuum space was set to be 15 Å to separate the interaction between periodic images. The climbing image nudged elastic band (NEB) method was used to calculate the energy barriers for decomposition of the H_2 molecule and diffusion of atomic H.[22,23]

RESULTS AND DISCUSSION

XPS spectra of two ZnO samples with Zn-terminated (0001) and O-terminated $(000\bar{1})$ surfaces were measured at room temperature with the pressure ranging from UHV to 1 and 0.5 mbar, respectively. The evolution of Zn $2p_{3/2}$ and O 1s peaks obtained from the two surfaces with changing H_2 pressure is shown in Figure 1a−d. Overall, with increasing H_2 pressure, the peaks from the $(000\bar{1})$ surface shifts to higher binding energy monotonically, while the peaks from the (0001) surface first shifts to lower binding energy and then turns to higher binding energy at about 0.05 mbar.

Figure 1e replots the peak positions of Zn $2p_{3/2}$ and O 1s as a function of H_2 pressure to better illustrate the distinct trends of the two polar surfaces. Regardless of the (0001) or $(000\bar{1})$ surface, only the shifts of whole XPS spectra were observed during a pressure cycle, suggesting that no additional chemical states were formed and only the charge transfer played the key role here.[24] Therefore, in Figure 1e, we take the peak positions under UHV condition as the reference. Here, the upshift on the $(000\bar{1})$ surface and the initial downshift followed by a sharp upturn on the (0001) surface can be clearly seen. The consistent trend of the Zn $2p_{3/2}$ and O 1s peaks suggests the reliability of the measurement and confirms that the peak shifts originate from charge transfer, which results in band bending at the surfaces. It is well known that the interfacial charge transfer can induce the depletion or accumulation of substrate charge carriers and hence the appearance of the surface band bending. If the interfacial charge transfer induces the electron depletion, the Fermi level moves away from the conduction band and an upward band bending occurs. As a consequence, the binding energies of the core-level peaks will be reduced. If the interfacial charge transfer induces the electron accumulation, the Fermi level moves closer to the conduction band (i.e., downward surface band bending), and the binding energies of the core-level peaks will be increased.[25]

We studied the reversibility of the phenomenon above by repeatedly varying the H_2 pressure. Figure 2a shows the evolutions of the Zn $2p_{3/2}$ and O 1s peaks on the (0001) surface during the pressure cycling. The XPS spectra are given

https://dx.doi.org/10.1021/acs.jpcc.0c08881
J. Phys. Chem. C 2020, 124, 25431−25436

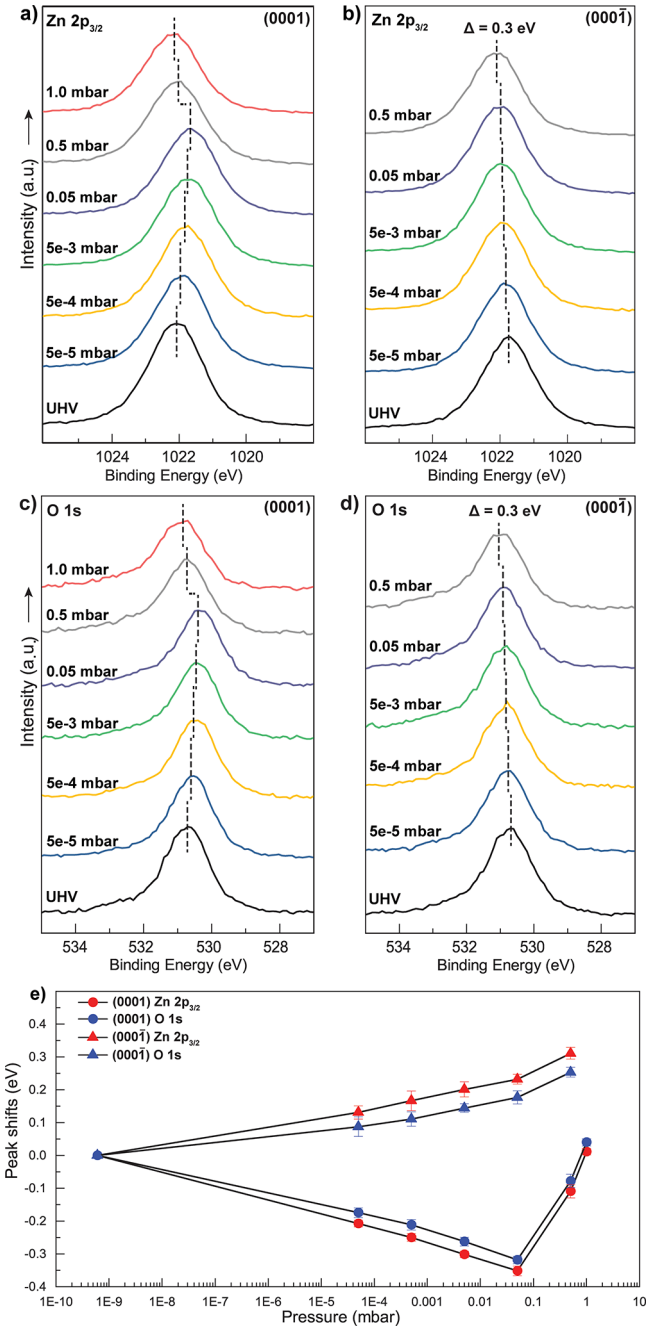

Figure 1. XPS spectra of Zn $2p_{3/2}$ from (a) ZnO(0001) and (b) ZnO(000$\bar{1}$) surfaces and spectra of O 1s from (c) ZnO(0001) and (d) ZnO(000$\bar{1}$) surfaces under different pressure of H_2. (e) Shifts of the peak positions of Zn $2p_{3/2}$ and O 1s as a function H_2 pressure on the two ZnO polar surfaces. The peak positions under UHV condition were taken as the reference.

in the Supporting Information (Figure S1). It can be seen that after pumping the H_2 gas out of the NAP cell, both peaks shift back to their original positions within an uncertainty of less than 0.05 eV, suggesting the reversibility of the chemical process that occurred on the (0001) surface. By increasing the H_2 pressure again, we observed the upturn of the peaks at nearly the same pressure range, suggesting the repeatability of this phenomenon. This pressure cycling experiment confirms that the interaction of H_2 with the (0001) surface is a reversible and pressure-dependent process.

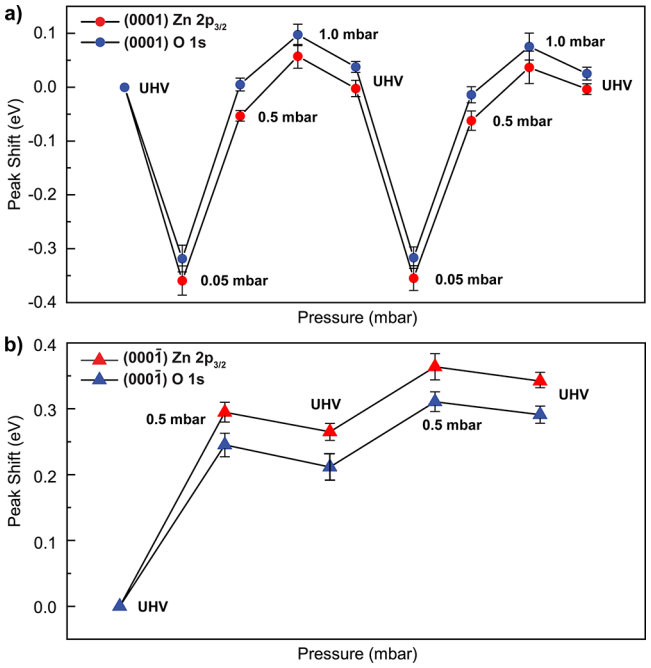

Figure 2. Pressure cycling experiment for studying the reversibility of Zn $2p_{3/2}$ and O 1s peak shifts under different pressures of H_2 as determined from NAP-XPS on (a) ZnO(0001) and (b) ZnO(000$\bar{1}$) surfaces.

Figure 2b shows the evolutions of the Zn $2p_{3/2}$ and O 1s peaks on the (000$\bar{1}$) surface during the pressure cycling. It can be seen that the interaction of H_2 with the (000$\bar{1}$) surface is distinctly different from the (0001) surface. Pumping the NAP cell to UHV again does not recover the XPS peak positions. Increasing the H_2 pressure again results in further shifts of the XPS peak positions toward higher binding energy. This result suggests that the interaction of H_2 with the (000$\bar{1}$) surface may be dissociative, and the adsorbed H species cannot escape from the surface once it is captured.

We carried out DFT calculations[18−20] to understand our NAP-XPS results. We first studied the adsorption configurations of H_2 molecule on both ZnO polar surfaces. The adsorption energy was calculated by $E_{ads} = E(H_2\text{-on-surf}) - E(\text{surf}) - E(H_2)$, where $E(H_2\text{-on-surf})$, $E(\text{surf})$, and $E(H_2)$ are the total energy for H_2 adsorbed on the surface, clean surface, and isolated H_2 molecule, respectively. The detailed results are summarized in the Supporting Information (Table S1, Figures S2−S7). We considered an H_2 molecule vertically or horizontally adsorbed on the hollow, top, and bridge sites. Our results show that the two polar surfaces do not exhibit significant difference regarding molecular H_2 adsorption. E_{ads} on the (0001) surface is −0.09 eV on the Zn-top site, while on the (000$\bar{1}$) surface, E_{ads} is −0.08 eV either on the Zn-top or bridge site. The interaction is typical physical adsorption because of van der Waals force. Considering the irreversible behavior on the (000$\bar{1}$) surface as observed in the NAP-XPS experiment, it is expected that H_2 dissociation occurs on the surfaces.

We further investigated the kinetics for H_2 dissociation on the two ZnO polar surfaces using the NEB method.[22,23] On the (0001) surface (Figure 3a), the energy barrier for H_2 dissociation is 0.23 eV, which could be readily overcome at room temperature. An equilibrium state with fully adsorbed atomic H on the (0001) surface could be quickly reached. On

https://dx.doi.org/10.1021/acs.jpcc.0c08881
J. Phys. Chem. C 2020, 124, 25431−25436

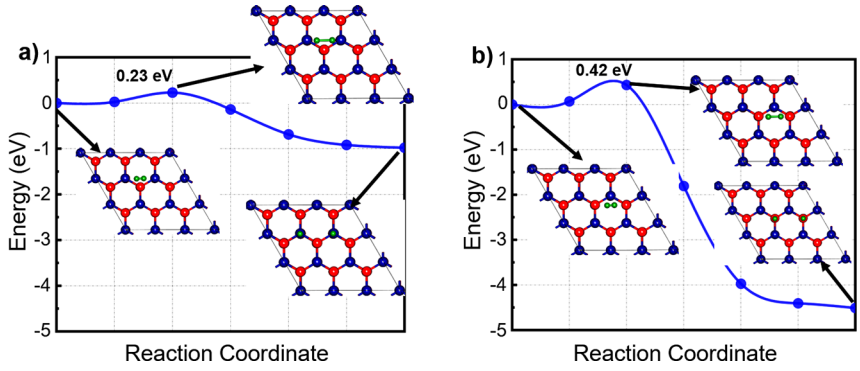

Figure 3. Energy profile for H_2 dissociation on (a) ZnO(0001) and (b) ZnO(000$\bar{1}$) surfaces obtained from NEB calculations. The insets show the atomic structures of the initial, final, and transition states. Zn atom (blue), O atom (red), and H atom (green).

the (000$\bar{1}$) surface (Figure 3b), the energy barrier for H_2 dissociation is 0.42 eV, suggesting a slower process than on the (000$\bar{1}$) surface but still achievable at room temperature. The slow dissociation may not saturate the surface coverage by atomic H in one pressure cycle. This could account for the further peak shift on the (000$\bar{1}$) surface in the second pressure cycle (Figure 2b).

From the NEB calculation, one can also obtain the H_2 dissociation energy, that is, the energy difference between the two ends of the energy profile. The dissociation energy on the (0001) surface is about 1.0 eV, while on the (000$\bar{1}$) surface, it is 4.5 eV. This result indicates that once the O−H bond is formed on the (000$\bar{1}$) surface, the OH-terminated (000$\bar{1}$) surface is rather stable, preventing H from escaping. The DFT results thus explain the irreversibility of the XPS peak shifts on the (000$\bar{1}$) surface after the system recovers to the UHV condition. Meanwhile, given the significantly smaller dissociation energy on the (0001) surface, the DFT results also provide a clue on the reversibility of the XPS peak shifts on the (0001) surface. However, the upturn of the peak shifts on this surface at high H_2 pressure is still a puzzle. Next, we carried out band structure calculation to understand the change of the electronic structure upon the exposure of H_2 with an aim of resolving this puzzle.

Figure 4a shows the band structure of the clean (0001) surface. Clearly, the dangling bonds of surface Zn atoms renders the Fermi level located in the conduction band about 1.6 eV above the CBM. When H_2 dissociation occurs and atomic H starts to gradually adsorb on the (0001) surface, the Fermi level shifts down. Figure 4b shows that when one H per supercell adsorbed on the surface corresponding to 1/4 ML coverage, the Fermi level shifts down to about 1.0 eV above the CBM. When the (0001) surface is half occupied by atomic H, the Fermi level moves into the band gap, as shown in Figure 4c. Apparently, the adsorbed H atom passivates the Zn dangling bond and acts as an acceptor. The acceptor behavior of adsorbed H results in positive charge accumulation near the surface, which results in the XPS peak shift to lower binding energy on the (0001) surface. The H adsorption on the (000$\bar{1}$) surface shows the opposite behavior to that on the (0001) surface. According to our DFT calculation, the movement of the Fermi level on the ZnO (000$\bar{1}$) surface always shows the same tendency regardless of the actual location of H (i.e., on the surface or at the subsurface). When H coverage is lower than one monolayer, the calculation further reveals that the formation energy of H at the subsurface is about 0.5 eV higher than that on the surface. Thus, the H atoms prefer to stay at

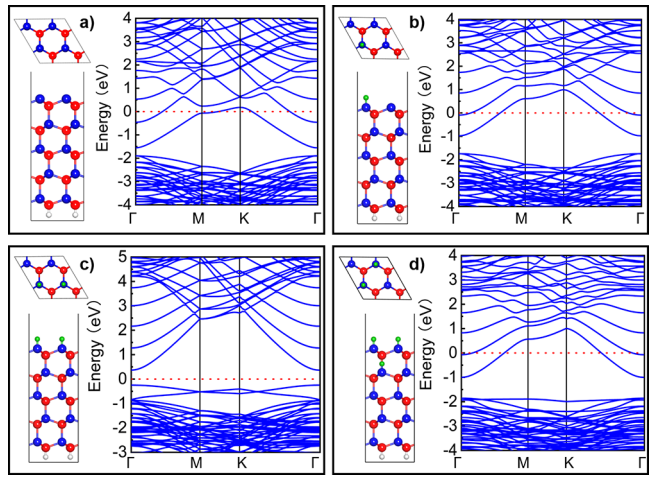

Figure 4. Top and side views of atomic structures of clean and H adsorbed ZnO(0001) surfaces and corresponding band structures. (a) 2 × 2 clean ZnO(0001) surface; (b) one H atom and (c) two H atoms adsorbed on the (0001) surface; (d) two H atoms adsorbed on the (0001) surface and the third H atom migrated into the subsurface. The dashed lines show the position of the Fermi level.

the surface to form OH^- rather than to diffuse into the subsurface to form interstitial H. The Fermi level on the clean surface is located in the valence band, while increasing the H coverage lifts the Fermi level up to the conduction band (Figure S8).

Our calculations show that when the H coverage is greater than half of the surface Zn sites, the H atom energetically prefers to diffuse into the bulk region, where the bond-center site shown in Figure 4d is the most stable site. The interstitial H in ZnO is well known to be a donor[26] and shifts the Fermi level upward to the conduction band. Note that the diffusion of H into the subsurface only occurs when the (0001) surface is saturated by adsorbed H. Based on the electron counting model,[27] each bulk Zn atom has four neighbours (O) and forms four bonds, so each Zn atom gives 0.5 electron to each bond to satisfy the octet rule. However, each surface Zn has three neighboring O; thus, each surface Zn has a dangling bond of 0.5 electron. In order to saturate the dangling bonds, every two Zn atoms will donor one electron to each adsorbed H atom on the surface. Therefore, the (0001) surface is fully saturated when H coverage is exactly 1/2 ML. If desorption of surface H occurs, the interstitial H in the bulk will migrate back to the surface. It is the dual stability and amphoteric behavior of atomic H (i.e., the ability to act as both a donor and an

https://dx.doi.org/10.1021/acs.jpcc.0c08881
J. Phys. Chem. C 2020, 124, 25431−25436

acceptor) depending on its position that is responsible for the pressure-dependent XPS peak shifts on the (0001) surface. To further demonstrate the amphoteric behavior of atomic H on the (0001) surface, we carried out Bader charge analysis[28] and found that each interstitial H in the bulk loses 0.66 electron, while on the surface, each receives 0.32 electron, confirming the donor and acceptor behavior, respectively, at the two sites.

CONCLUSIONS

In summary, the reaction of H_2 with the ZnO polar surfaces was investigated by NAP-XPS at varying H_2 pressures up to 1 mbar. On the O-terminated $(000\bar{1})$ surface, the XPS peaks shift to higher binding energy with increasing H_2 pressure and the shift is irreversible. In contrast, on the Zn-terminated (0001) surface, the XPS peaks shift to lower binding energy first and then turn to higher binding energy when the H_2 pressure is above 0.05 mbar. The process on the (0001) surface is found to be reversible. DFT calculations were conducted to understand the observed polarity- and pressure-dependent hydrogen dynamics. It is found that on both surfaces, H_2 adsorption is dissociative. The dissociation barrier and dissociation energy on the (0001) surface are significantly lower than those on the $(000\bar{1})$ surface, resulting in faster dissociation kinetics and reversible adsorption/desorption on the (0001) surface. Atomic H on the (0001) and $(000\bar{1})$ surfaces exhibits acceptor and donor behavior, respectively, which accounts for the opposite trends of XPS peak shifts at low H_2 pressure. The upturn of the peak shift on the (0001) surface at high H_2 pressure is attributed to migration of atomic H to the subsurface, where the interstitial H acts as the donor.

ASSOCIATED CONTENT

Supporting Information

The Supporting Information is available free of charge at https://pubs.acs.org/doi/10.1021/acs.jpcc.0c08881.

Adsorption energy for H and H_2 on ZnO polar surfaces, NAP-XPS spectra of ZnO polar surfaces under H_2, structure of H or H_2 absorbed on ZnO polar surfaces, and atomic structures of clean and H adsorbed ZnO $(000\bar{1})$ surfaces and corresponding band structures (PDF)

AUTHOR INFORMATION

Corresponding Authors

Kaidi Yuan − *School of Physical Science and Technology, ShanghaiTech University, Shanghai 201210, China*; Email: yuankd@shanghaitech.edu.cn

Yi-Yang Sun − *State Key Laboratory of High Performance Ceramics and Superfine, Microstructure, Shanghai Institute of Ceramics, Chinese Academy of Sciences, Shanghai 201899, China*; orcid.org/0000-0002-0356-2688; Email: yysun@mail.sic.ac.cn

Wei Chen − *Department of Chemistry and Department of Physics, National University of Singapore, 117543, Singapore; Joint School of National University of Singapore and Tianjin University, Fuzhou 350207, China*; orcid.org/0000-0002-1131-3585; Email: phycw@nus.edu.sg

Authors

Zhirui Ma − *Department of Chemistry, National University of Singapore, 117543, Singapore*; orcid.org/0000-0002-1381-7752

Ke Yang − *Department of Physics, Applied Physics & Astronomy, Rensselaer Polytechnic Institute, Troy, New York 12180, United States; Department of Applied Physics, School of Physics and Electronics, Hunan University, Changsha 410082, China*

Xu Lian − *Department of Chemistry and Center for Advanced 2D Materials, National University of Singapore, 117543, Singapore*; orcid.org/0000-0003-1736-6247

Shuo Sun − *Department of Chemistry, National University of Singapore, 117543, Singapore*; orcid.org/0000-0001-6092-7148

Chengding Gu − *Department of Chemistry, National University of Singapore, 117543, Singapore*; orcid.org/0000-0003-1555-2601

Jia Lin Zhang − *Department of Chemistry, National University of Singapore, 117543, Singapore*; orcid.org/0000-0002-6130-2294

Damien West − *Department of Physics, Applied Physics & Astronomy, Rensselaer Polytechnic Institute, Troy, New York 12180, United States*; orcid.org/0000-0002-4970-3968

Shengbai Zhang − *Department of Physics, Applied Physics & Astronomy, Rensselaer Polytechnic Institute, Troy, New York 12180, United States*

Lei Liu − *State Key Laboratory of Luminescence and Applications, Changchun Institute of Optics, Chinese Academy of Sciences, Changchun 130033, China*; orcid.org/0000-0002-9714-2130

Hexing Li − *Key Laboratory of Resource Chemistry of Ministry of Education, College of Chemistry and Materials Science, Shanghai Normal University, Shanghai 200234, China*; orcid.org/0000-0002-3558-5227

Complete contact information is available at: https://pubs.acs.org/10.1021/acs.jpcc.0c08881

Author Contributions

Z.M. and K.Y. contributed equally. The manuscript was written through contributions of all authors. All authors have given approval to the final version of the manuscript.

Notes

The authors declare no competing financial interest.

ACKNOWLEDGMENTS

The authors acknowledge the financial support from the National Natural Science Foundation of China (grant no. 91645102), Singapore National Research Foundation under the grant of NRF2017NRF-NSFC001-007, and NUS Flagship Green Energy Programme. K.Y. thanks the China Scholarship Council (CSC) for financial support.

REFERENCES

(1) Gawande, M. B.; Pandey, R. K.; Jayaram, R. V. Role of Mixed Metal Oxides in Catalysis Science—Versatile Applications in Organic Synthesis. *Catal. Sci. Technol.* **2012**, *2*, 1113−1125.

(2) Lwin, S.; Wachs, I. E. Olefin Metathesis by Supported Metal Oxide Catalysts. *ACS Catal.* **2014**, *4*, 2505−2520.

(3) Kattel, S.; Ramírez, P. J.; Chen, J. G.; Rodriguez, J. A.; Liu, P. Active Sites for CO_2 Hydrogenation to Methanol on Cu/ZnO Catalysts. *Science* **2017**, *355*, 1296−1299.

(4) Kuld, S.; Thorhauge, M.; Falsig, H.; Elkjaer, C. F.; Helveg, S.; Chorkendorff, I.; Sehested, J. Quantifying the Promotion of Cu Catalysts by ZnO for Methanol Synthesis. *Science* **2016**, *352*, 969−974.
(5) Galván, C. Á.; Schumann, J.; Behrens, M.; Fierro, J. L. G.; Schlögl, R.; Frei, E. Reverse Water-gas Shift Reaction at the Cu/ZnO Interface: Influence of the Cu/Zn Ratio on Structure-activity Correlations. *Appl. Catal., B* **2016**, *195*, 104−111.
(6) Jiao, F.; Li, J.; Pan, X.; Xiao, J.; Li, H.; Ma, H.; Wei, M.; Pan, Y.; Zhou, Z.; Li, M.; Miao, S.; Li, J.; Zhu, Y.; Xiao, D.; He, T.; Yang, J.; Qi, F.; Fu, Q.; Bao, X. Selective Conversion of Syngas to Light Olefins. *Science* **2016**, *351*, 1065−1068.
(7) Lunkenbein, T.; Schumann, J.; Behrens, M.; Schlögl, R.; Willinger, M. G. Formation of a ZnO Overlayer in Industrial Cu/ZnO/Al_2O_3 Catalysts Induced by Strong Metal−Support Interactions. *Angew. Chem., Int. Ed.* **2015**, *54*, 4544−4548.
(8) Wöll, C. The Chemistry and Physics of Zinc Oxide Surfaces. *Prog. Surf. Sci.* **2007**, *82*, 55−120.
(9) Wang, Y.; Meyer, B.; Yin, X.; Kunat, M.; Langenberg, D.; Traeger, F.; Birkner, A.; Wöll, C. Hydrogen Induced Metallicity on the ZnO (1010) Surface. *Phys. Rev. Lett.* **2005**, *95*, 266104.
(10) Meyer, B. First-principles Study of the Polar O-terminated ZnO Surface in Thermodynamic Equilibrium with Oxygen and Hydrogen. *Phys. Rev. B: Condens. Matter Mater. Phys.* **2004**, *69*, 045416.
(11) Becker, T.; Hövel, S.; Kunat, M.; Boas, C.; Burghaus, U.; Wöll, C. Interaction of Hydrogen with Metal Oxides: the Case of the Polar ZnO (0 0 0 1) Surface. *Surf. Sci.* **2001**, *486*, L502−L506.
(12) Chen, H.; Lin, L.; Li, Y.; Wang, R.; Gong, Z.; Cui, Y.; Li, Y.; Liu, Y.; Zhao, X.; Huang, W.; Fu, Q.; Yang, F.; Bao, X. CO and H_2 Activation over g-ZnO Layers and w-ZnO (0001). *ACS Catal.* **2019**, *9*, 1373−1382.
(13) Porsgaard, S.; Jiang, P.; Borondics, F.; Wendt, S.; Liu, Z.; Bluhm, H.; Besenbacher, F.; Salmeron, M. Charge State of Gold Nanoparticles Supported on Titania under Oxygen Pressure. *Angew. Chem., Int. Ed.* **2011**, *50*, 2266−2269.
(14) Yuan, K.; Zhong, J.-Q.; Sun, S.; Ren, Y.; Zhang, J. L.; Chen, W. Reactive Intermediates or Inert Graphene? Temperature- and Pressure-Determined Evolution of Carbon in the CH4−Ni (111) System. *ACS Catal.* **2017**, *7*, 6028−6037.
(15) Yuan, K.; Zhong, J.-Q.; Zhou, X.; Xu, L.; Bergman, S. L.; Wu, K.; Xu, G. Q.; Bernasek, S. L.; Li, H. X.; Chen, W. Dynamic Oxygen on Surface: Catalytic Intermediate and Coking Barrier in the Modeled CO_2 Reforming of CH_4 on Ni (111). *ACS Catal.* **2016**, *6*, 4330−4339.
(16) Bruno, G.; Michela, G. M.; Graziella, M.; Pio, C.; Ignazio, L. F.; Maria, L. Is There a ZnO Face Stable to Atomic Hydrogen? *Adv. Mater.* **2009**, *21*, 1700−1706.
(17) Ozawa, K.; Mase, K. Metallization of ZnO ($10\bar{1}0$) by Adsorption of Hydrogen, Methanol, and Water: Angle-resolved Photoelectron Spectroscopy. *Phys. Rev. B: Condens. Matter Mater. Phys.* **2010**, *81*, 205322.
(18) Blöchl, P. E. Projector Augmented-wave Method. *Phys. Rev. B: Condens. Matter Mater. Phys.* **1994**, *50*, 17953−17979.
(19) Kresse, G.; Furthmüller, J. Efficiency of Ab-initio Total Energy Calculations for Metals and Semiconductors using a Plane-wave Basis Set. *Comput. Mater. Sci.* **1996**, *6*, 15−50.
(20) Kresse, G.; Furthmüller, J. Efficient Iterative Schemes for Ab Initio Total-energy Calculations using a Plane-wave Basis Set. *Phys. Rev. B: Condens. Matter Mater. Phys.* **1996**, *54*, 11169−11186.
(21) Perdew, J. P.; Ruzsinszky, A.; Csonka, G. I.; Vydrov, O. A.; Scuseria, G. E.; Constantin, L. A.; Zhou, X.; Burke, K. Restoring the Density-Gradient Expansion for Exchange in Solids and Surfaces. *Phys. Rev. Lett.* **2008**, *100*, 136406.
(22) Henkelman, G.; Uberuaga, B. P.; Jónsson, H. A Climbing Image Nudged Elastic Band Method for Finding Saddle Points and Minimum Energy Paths. *J. Chem. Phys.* **2000**, *113*, 9901−9904.
(23) Henkelman, G.; Jónsson, H. Improved Tangent Estimate in the Nudged Elastic Band Method for Finding Minimum Energy Paths and Saddle Points. *J. Chem. Phys.* **2000**, *113*, 9978−9985.
(24) Tosi, E.; Comedi, D.; Zampieri, G. Band Bending at the ZnO (0001)-Zn Surface Produced by Electropositive, Electronegative and Atmospheric Adsorbates. *Appl. Surf. Sci.* **2019**, *495*, 143592.
(25) Zhang, Z.; Yates, J. T. Band Bending in Semiconductors: Chemical and Physical Consequences at Surfaces and Interfaces. *Chem. Rev.* **2012**, *112*, 5520−5551.
(26) Van de Walle, C. G. Hydrogen as a Cause of Doping in Zinc Oxide. *Phys. Rev. Lett.* **2000**, *85*, 1012.
(27) Pashley, M. D. Electron Counting Model and its Application to Island Structures on Molecular-beam Epitaxy Grown GaAs (001) and ZnSe (001). *Phys. Rev. B: Condens. Matter Mater. Phys.* **1989**, *40*, 10481.
(28) Yu, M.; Trinkle, D. R. Accurate and Efficient Algorithm for Bader Charge Integration. *J. Chem. Phys.* **2011**, *134*, 064111.

https://dx.doi.org/10.1021/acs.jpcc.0c08881
J. Phys. Chem. C 2020, 124, 25431−25436